

SHORT CYCLIC STRUCTURES IN POLYMER MODEL NETWORKS: A TEST OF MEAN FIELD APPROXIMATION BY MONTE CARLO SIMULATIONS

M. LANG, K. SCHWENKE, AND J.-U. SOMMER

ABSTRACT. A mean field rate theory description of the homo- and co-polymerization of f -functional molecules is developed, which contains the formation of short cyclic structures inside the network. The predictions of this model are compared with Monte-Carlo simulations of cross-linking of star polymers in solution. We find that homo-polymerizations are well captured by mean-field models at concentrations larger than one quarter of the geometrical overlap concentration. All simulation data can be fit using a single geometric parameter for cyclization. The simulation data reveal that within the range of parameters of the present study correlations among multiply connected molecules can be neglected. Thus, mean-field treatments of homopolymerizations are reasonable approximations, if short cycles are properly addressed. Co-polymerization is considered in the case of strict A-B reactions, where all reactive groups of individual molecules are either of type A or B. For these systems we find a clear influence of the local intermixing of A and B groups for all concentrations investigated. In consequence, mean-field models are less appropriate to describe the simulation data. The lack of ring structures containing an odd number of molecules as compared to homopolymerizations at same extent of reaction allows for the formation of stable AB networks at concentrations one order of magnitude below the geometrical overlap concentration.

1. INTRODUCTION

Cyclization during stepwise polymerization is a still incompletely understood problem. While there are clear experimental data and well accepted theoretical models for systems resulting in linear chains and rings, the situation is much more complicated for network forming reactions [24]. There, only indirect experimental measures for the amount of ring formation inside the gel are available: for instance, the weight distribution of sol or the shift in the gel point can be used to estimate the degree of cyclization inside the gel [30]. Both methods require a theoretical model based upon several assumptions to extract the degree of cyclization from the available data. Therefore, a rigorous quantitative description of the processes of branched polycondensation with allowance of intramolecular reactions is not yet available [8].

Computer simulations, on the other hand, allow to directly analyze the degree of cyclization for any cross-linking reaction. Therefore, a large number of simulation works in the past focused on

the effect of cyclization as summarized in [30, 12]. While dynamic simulations of network formation mainly concentrate on the total amount of cycles or the shortest cycles in the sample, the data focusing on critical dilution was obtained either by experiments or static simulations of a percolating lattice. A simulation study that includes the dynamics of the molecules and thus, incorporates the effects of flocculation at concentrations towards critical dilution, however, is still lacking.

In general, any theoretical description of network formation is founded on several assumptions concerning the reaction mechanism, the motion of polymers, mixing of different species, etc ..., which are difficult to test by experiments [8]. Since computer simulations can model these effects and allow for a detailed analysis, a critical test of the assumptions underlying the theoretical models is of great importance, but still remains incomplete in previous works [12, 13, 15, 31].

As reviewed in [8], there are several approaches for a theoretical treatment of the problem of cyclization. Spanning tree models [24, 7, 23, 5, 4] essentially treat ring forming reactions by assigning pairs of unreacted sites inside the branched molecules. This assignment is typically based upon estimating the return probability of Gaussian chains or branched structures with Gaussian conformations. Conformational changes upon ring formation and correlations among rings are usually neglected and the total effect of ring formation is expressed in a shift of the total conversion. Beyond the gel point, this general scheme is no more applicable, since the probability for ring formation is equal to one within this approach, while the actual rate of intramolecular reactions is rather proportional to the square number fraction of reactive groups inside the gel. Sarmoria et al. [23] therefore suggest three different models that circumvent this problem, but due to the lack of suitable experimental or simulation data, it is difficult to decide, which model might be the best approximation for real systems.

Rate theories [27, 28] use a set of differential equations that describe the transition among different species in the reaction container. The advantage of this method is that it is exact within a mean-field approach and that it allows to model any correlation among the particular molecular species or conformational changes induced by cyclization. It has been shown [12], that the predictions of rate theories and spanning tree models or the work of Suematsu [30] are consistent with simulation data and among each other at low degrees of cyclization [8, 12]. But as a mean-field treatment, such methods are not sensitive to fluctuations. Thus, a cross-test of rate theory (or any other equivalent mean-field approach) with computer simulations of network formation that explicitly models mixing, dynamics, and fluctuations would be important for testing the applicability of mean-field models

to the problem of cyclization inside a gel. This test will be most critical at high rates of loop formation at or below the overlap concentration. Therefore, we study in the present work the rates of cyclization as function of concentration and compare with rate theory predictions in which we incorporate all necessary information on molecular conformations, concentrations, mixing, and connectivity of the molecules.

As model systems we discuss the homopolymerization and co-polymerization of structurally identical f -functional molecules. The latter is the simplest example of reacting molecules that are subject to composition fluctuations of reactive groups of different type. As further simplification we investigate star-shaped molecules with arms of equal degree of polymerization $N_a = N/f$, where N is the degree of polymerization of the molecule. Recently, T. Sakai *et al.* synthesized hydrogels made of 4-arm star polymers with tetra-Nhydroxysuccinimide-glutarate-terminated PEG (A-type) and tetraamine-terminated PEG (B-type) as precursor molecules, “Tetra-PEG-gels” [22]. These gels, which showed remarkable mechanical properties, should have a structure equivalent to the co-polymer model networks of our study.

This work is structured as follows. First, we discuss the reaction rates used to model gelation. Then, we compute the distribution of species concerning connectivity inside the evolving network. The network properties are estimated based on a simplified phantom model picture. All theoretical predictions are compared with the simulation data obtained by cross-linking simulations of solutions of star molecules as described in the previous paper [26]. Note that these simulations explicitly model dynamics and conformations of all molecules or clusters of molecules during cross-linking. Furthermore, excluded volume, the concentration dependence of chain conformations, and network elasticity is explicitly modeled, which is a clear advantage over previous simulation studies on cyclization in networks [16, 2, 29]. The main parameters of the simulation data we have to keep in mind are that a) all reactions were stopped close to 95% conversion of the reactive groups, b) all data is for 4-functional stars and c) all data is always represented as function of concentration c with respect to overlap concentration c^* . Therefore, all theoretical computations below use the same conversion $p = 0.95$ for comparison, which is close to previous NMR results [14]. As in previous works [31, 12, 10], we did not observe significant modifications (except of some weak deviations for AB networks at $p > 0.9$) of network structure as function of the reactivity of the molecules. Therefore, we compare the data of the present study that is obtained at reaction probability one (limit of diffusion-controlled reactions) with theoretical predictions that are derived for equilibrium

reactions at infinitely low reaction rate (limit of reaction-controlled reactions) without any further corrections. In order to eliminate time dependencies, all data and theory is presented as function of conversion. Note that the overlap concentration c^* is determined by a geometrical analysis of chain conformations as described in ref [26].

2. REACTION RATES

First, we develop a notation scheme that allows to distinguish any possible local connectivity of a given f -functional molecule. Throughout this work we restrict the analysis to nearest neighbour connections inside the gel. Therefore, only cyclic structures containing one or two molecules are distinguished from all remaining connections. Let R_i denote that a molecule is attached to a ring containing i molecules. Similarly we use R_i^j to describe that the molecule is part of j rings of size i , whereby we distinguish between different neighbours for ring formation. Thus, $R_2R_2 \neq R_2^2$, since the former describes two “double links” R_2 with two *different* neighbours, while the latter is a “triple link” with the *same* neighbour, see Figure 2.1 for more details. I_j describes an f -functional star that forms j “ideally” branching connections; not yet connected groups are not denoted. All available information on the connectivity of a given star as shown in Figure 2.1 is summarized in the notation R_1R_2 , R_1I_2 , etc ...,.. Note that throughout this section we consider only number fractions of species among all stars. Thus, the star connectivity R_1R_2 simultaneously denotes the number fraction of stars with exactly this connectivity.

Let us also introduce reaction rates $k_{l,m}$ to describe irreversible transitions among the different possible connectivities of the stars. Here, the index l is 0, if the reaction is ideally branching, or equal to i , if a ring of i molecules is formed. The index $m = 0, \dots, f - 1$ denotes the number of reacted groups at the molecules for $l = 0, 1$ and the number of existing bonds between the given pair of stars for $l = 2$, see Figure 2.1 and equations (3.1) to (3.17) for more details.

For deriving the rate constants among the different transitions we use the following rules:

- a) All reaction rates are estimated based upon local concentrations of the particular pairs of reactive groups.
- b) Reactions among previously unconnected groups are independent of each other.
- c) Reactions among previously connected groups depend on the equilibrium conformations of the structure between the reactive groups.

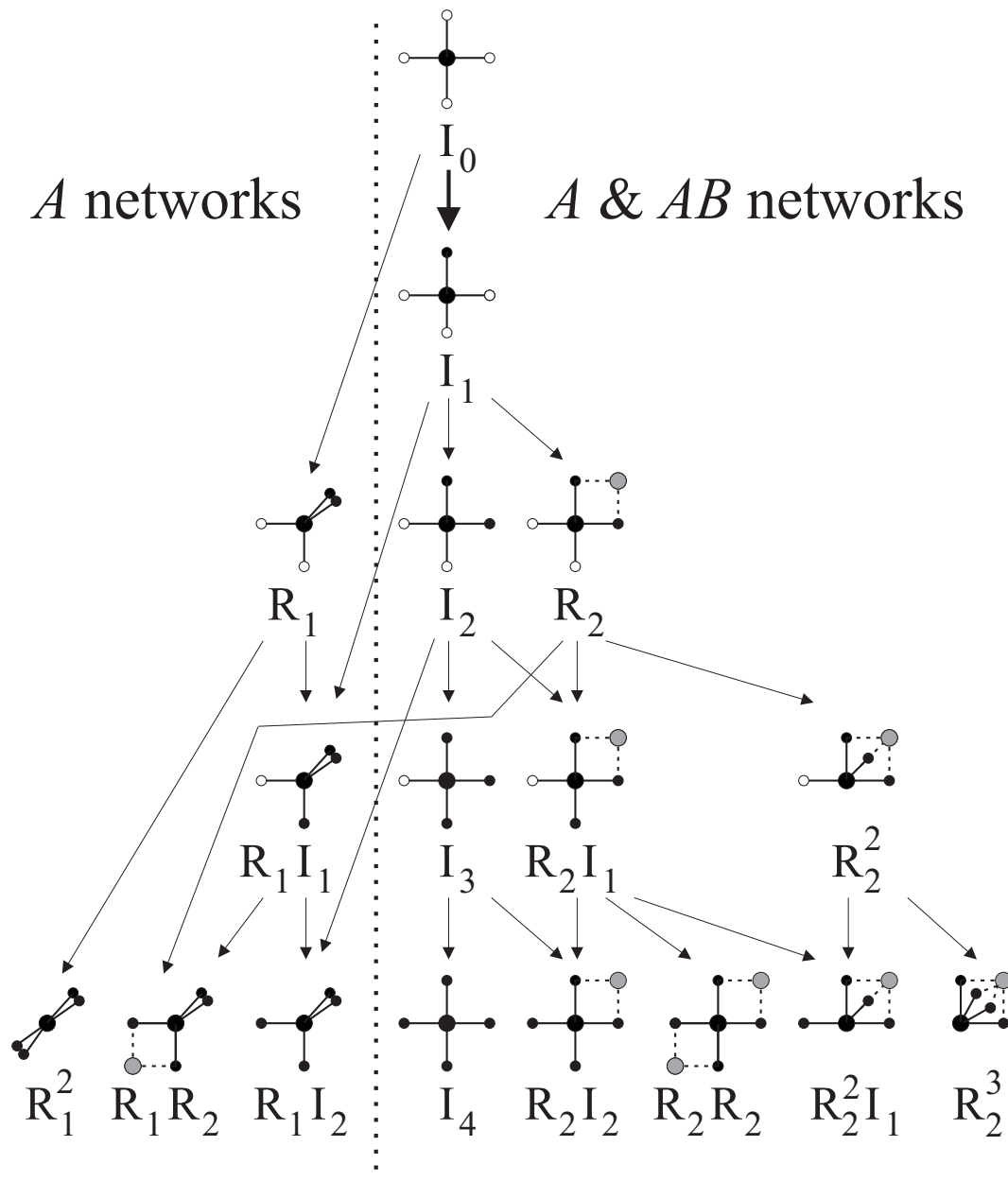


FIGURE 2.1. Reaction diagram: f -functional molecules (stars) are depicted by their centers (large black circles) and their unreacted (small white circles) and reacted (small black circles) groups that can form multiple connections to neighboring stars (grey circles). Star arms are shown by black lines, arms of neighboring stars by dashed lines. The arrows indicate the possible irreversible reactions.

For the *ideally branching reactions* we assume that the reaction rate of a given reactive group is proportional to the average concentration of all reactive groups at unconnected stars, which is approximately $cf(1 - p)$. Here, cf is the initial concentration of reactive groups and p the fraction of reacted groups. Since in the present work we only consider connections up to next neighbours,

this approximation is also applicable beyond the gel point [10]. The reaction rate of a star with $f - m$ unreacted groups is then given by

$$(2.1) \quad k_{0,m}(c) = cf(f - m)(1 - p).$$

For the above equation (and the equations below) we implicitly assume that steric repulsion among reactive groups can be neglected, which is a reasonable approximation for stars of small f . Networks of large f will require an improvement of the above equation.

The *formation of loops* R_1 is computed by estimating the concentration of pairs of unreacted groups inside a star. For $c > c^*$, the star conformation changes as function of concentration as discussed in our previous work [26], and thus, the rate of collisions between two reactive groups of a star depends on the size of the star

$$(2.2) \quad k_{1,m}(c > c^*) \approx k_{1,m}(c^*) \cdot (c/c^*)^{-\beta}.$$

We find $\beta \approx 0.65$, if we only consider the concentration dependence of star conformations. A best fit of the loop data for $c > c^*$ reveals $\beta \approx 0.53$, which might be caused by an additional effect of desinterpenetration of stars, since also the shape of the correlation hole of the star centers changes as function of concentration [26]. For $c < c^*$ we assume that the conformation of the star and thus, the frequency of collisions inside the star remain unchanged as function of concentration:

$$(2.3) \quad k_{1,m}(c < c^*) \approx k_{1,m}(c^*).$$

The frequency of collisions of reactive groups inside a star at a given concentration c is proportional to the number of distinguishable pairs of arms and the single pair reaction rate $k_{1,f-2}(c)$,

$$(2.4) \quad k_{1,m}(c) = \binom{f - m}{2} k_{1,f-2}(c)$$

which we denote using a binomial coefficient for the number of pairs of unreacted arms.

At the geometrical overlap concentration $c = c^*$ and at the beginning of the reaction, $p = 0$, we fix the ratio of single pair intra-molecular reactions $k_{1,f-2}$ and ideal reactions of a single reactive group, $k_{0,f-1}$, by comparing the concentrations of the reaction partners

$$(2.5) \quad \frac{k_{1,f-2}(c^*)}{k_{0,f-1}(c^*)} \approx \frac{R_g^3}{R_e^3}.$$

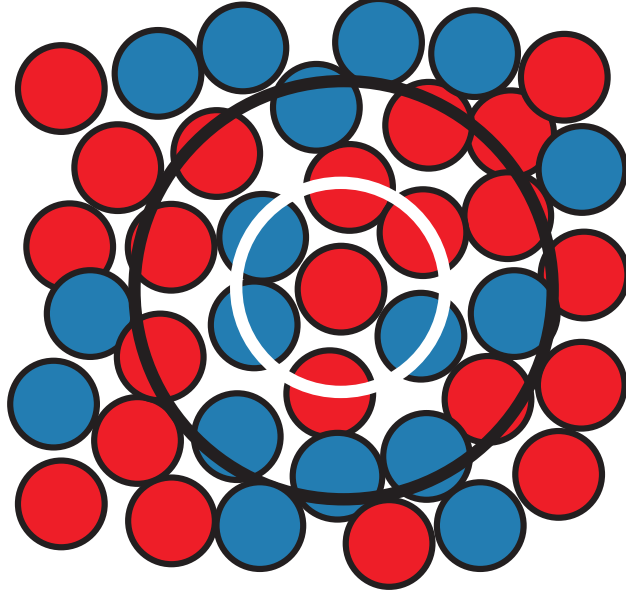


FIGURE 2.2. The gyration volumes R_g^3 densely fill space near c^* . Stars of different type are displayed in different color. The white circle indicates the volume R_e^3 from which reactive groups are selected for reaction, the black shows the range within the centers of mass of possible reaction partners must be located.

This relation reflects that the geometrical overlap condition is determined from changes in R_g , while reactions can occur within the volume that is accessible to the ends groups attached to the arms of the stars, see Figure 2.2. If we use the ideal prediction for $R_g^2 = (3 - 2/f) \cdot N_a b^2/6$ and estimate $R_e \approx 2^{1/2} N_a$, we find an additional geometrical prefactor of approximately 6/5 for the present case of 4-arm stars in order to fit the simulation data on the formation of loops R_1 . We note that R_g^3/R_e^3 as computed by theory or by directly taking the simulation data differ by less than 2% for $N \geq 16$. Therefore, the prefactor of approximately 6/5 must be attributed to the partial disinterpenetration of the stars at c^* due to excluded volume interactions between stars. This is also sketched at Figure 2.2: repulsion and disinterpenetration among stars occurs up to R_g , while reaction partners are selected via the endgroups on a larger distance as indicated by the white circle.

The *reaction rates for loops* R_2 are estimated by computing the concentrations of *pairs* of reactive groups among two different connected stars. For any star we know the functionality f , the number of reacted groups m , the number of different connected stars $b \leq m$, and the number n of bonds to a particular connected star. The missing information is the average number of unreacted groups b_n at each connected star, if there are n bonds connecting to this star for computing the number of unreacted pairs that form loops R_2 . Here, b_n is derived from the reaction diagram by considering

that any star is selected proportional to the weight fraction of its reacted arms (or pairs of arms, if there are multiple connections). The expected number of unreacted groups can be written as

$$(2.6) \quad b_1 = (3 \cdot I_1 + 4 \cdot I_2 + 3 \cdot I_3 + R_1 I_1 + R_2 I_1) / \left(\sum_{k=1}^f k \cdot I_k + R_1 I_1 + R_2 I_1 + 2 \cdot R_1 I_2 + 2 \cdot R_2 I_2 + 2 R_2 I_1 \right),$$

$$(2.7) \quad b_2 = \frac{2 \cdot R_2 + R_2 I_1}{R_2 + R_2 I_1 + 2 \cdot R_2 R_2 + R_2 I_2 + R_2 R_1},$$

$$(2.8) \quad b_3 = \frac{R_2^2}{R_2^2 + 2 R_2 I_1}.$$

The denominator in the three equations above contains all star connectivities that can be connected with a given star by n bonds between both molecules, while the numerator contains only that fraction of connectivities that contains at least one unreacted group multiplied by the particular number of unreacted groups.

The average distance between the star centers is reduced with increasing number n of connections between the stars. Assuming random walk conformations and Gaussian elasticity of strands, loop formation is additionally proportional to $[(1 + 1/n)/2]^{-3/2}$. Thus, we find

$$(2.9) \quad k_{2,n}(c) = 2^{-3/2} b_n [(1 + 1/n)/2]^{-3/2} k_{1,f-2}(c),$$

which we define here for a single unreacted group at the selected star and one connected star using n bonds. Note that the proper concentration dependence enters implicitly via the concentration dependence of $k_{1,f-2}$.

For some star connectivities, the particular number of connected stars with n bonds and the numbers of unreacted groups $f-m$ is different from one. This is then explicitly denoted as individual prefactor of the rates $k_{2,n}$ at equations (3.10) to (3.17)¹.

With the above set of equations we can compute the ratios among all rate constants as function of conversion, and thus, the problem can always be solved by numerical integration. Note that above only the ratio of $k_{1,f-2}(c^*)/k_{0,f-1}(c^*)$ (i.e. single pair intra-molecular vs. single pair inter-molecular reaction rate) has to be fixed by comparison with the simulation data. All other reaction

¹For instance, the connectivity I_2 has two single connections and two unreacted groups, which leads to an extra factor of 4 for $k_{2,1}$ at equation 3.3.

rates are computed as multiples of either $k_{1,f-2}$ or $k_{0,f-1}$, and thus, this ratio is the *only* adjustable parameter for all computations.

There is a large body of works that derive rate equations similar to our discussion above as summarized, for instance, in the review of Kuchanov [8]. The largest overlap exists with the work of Dusek [5] and Sarmoria et al. [19, 24, 23]. Because of computing expectation values for the intra-molecular reactions (equations 2.6 - 2.8) our approach is formally equivalent to model A of [23]. The main differences to the present work are a) the work of Sarmoria et al. does not consider conformational changes of the polymers upon dilution, b) conformational changes due to the formation of cycles are also neglected (cf. equation 2.9), and c) the spanning tree approximation is problematic beyond the gel point [23], while the approach of the present work investigates rings of short length and thus, does not suffer from a diverging fraction of intramolecular reactions. The limitation to short cycles is clearly problematic close to the gel point, however, the comparison with the simulation data will show that our approximation is sufficient for well-developed networks at essentially all experimentally important concentrations.

Note that for a discussion of samples close to the gel point, the set of rate constants above can be readily extended to incorporate cycles of larger size up to critical generation i_c at which there is the transition from mainly branching structures to a 3d-like behaviour of the network structure [10]. The approach breaks down when modeling cyclic structures containing more than $i \geq i_c$ molecules, since the contribution of intramolecular reactions is diverging. We also have to clarify that our work represents an enhanced mean-field approach that aims to correctly approximate the effects of cycles in the networks, but does not consider fluctuations of any kind. Therefore, it can only be applied as reasonable approximation outside of the Ginzburg zone around the critical point [21].

3. RATE EQUATIONS FOR STAR CONNECTIVITIES

For comparing simulation data and theory, we integrate here with respect to conversion. Let dp be an infinitesimal change in conversion p . Using the above reaction rates we obtain for $f = 4$ for the entirely branching units I_i

$$(3.1) \quad \frac{dI_0}{dp} = -(k_{0,0} + k_{1,0})I_0$$

$$(3.2) \quad \frac{dI_1}{dp} = k_{0,0}I_0 - (k_{0,1} + k_{1,1} + 3 \cdot k_{2,1})I_1$$

$$(3.3) \quad \frac{dI_2}{dp} = k_{0,1}I_1 - (k_{0,2} + k_{1,2} + 4 \cdot k_{2,1})I_2$$

$$(3.4) \quad \frac{dI_3}{dp} = k_{0,2}I_2 - (k_{0,3} + 3 \cdot k_{2,1})I_3$$

$$(3.5) \quad \frac{dI_4}{dp} = k_{0,3}I_3.$$

For the stars containing branching connections I_i and loops R_1 we get

$$(3.6) \quad \frac{dR_1}{dp} = k_{1,0}I_0 - (k_{0,2} + k_{1,2})R_1$$

$$(3.7) \quad \frac{dR_1I_1}{dp} = k_{1,1}I_1 + k_{0,2}R_1 - (k_{0,3} + k_{2,1})R_1I_1$$

$$(3.8) \quad \frac{dR_1I_2}{dp} = k_{0,3}R_1I_1 + k_{1,2}I_2$$

$$(3.9) \quad \frac{dR_1^2}{dp} = k_{1,2}R_1,$$

for the stars containing branching connections I_i and loops R_2

$$(3.10) \quad \frac{dR_2}{dp} = 3 \cdot k_{2,1}I_1 - (k_{0,2} + k_{1,2} + k_{2,2})R_2$$

$$(3.11) \quad \frac{dR_2I_1}{dt} = k_{0,2}R_2 + 4 \cdot k_{2,1}I_2 - (k_{0,3} + k_{2,1} + k_{2,2})R_2I_1$$

$$(3.12) \quad \frac{dR_2^2}{dp} = k_{2,2}R_2 - (k_{0,3} + k_{2,3})R_2^2$$

$$(3.13) \quad \frac{dR_2I_2}{dp} = k_{0,3}R_2I_1 + 3 \cdot k_{2,1}I_3$$

$$(3.14) \quad \frac{dR_2R_2}{dp} = k_{2,1}R_2I_1$$

$$(3.15) \quad \frac{dR_2^2I_1}{dp} = k_{0,3}R_2^2 + k_{2,2}R_2I_1$$

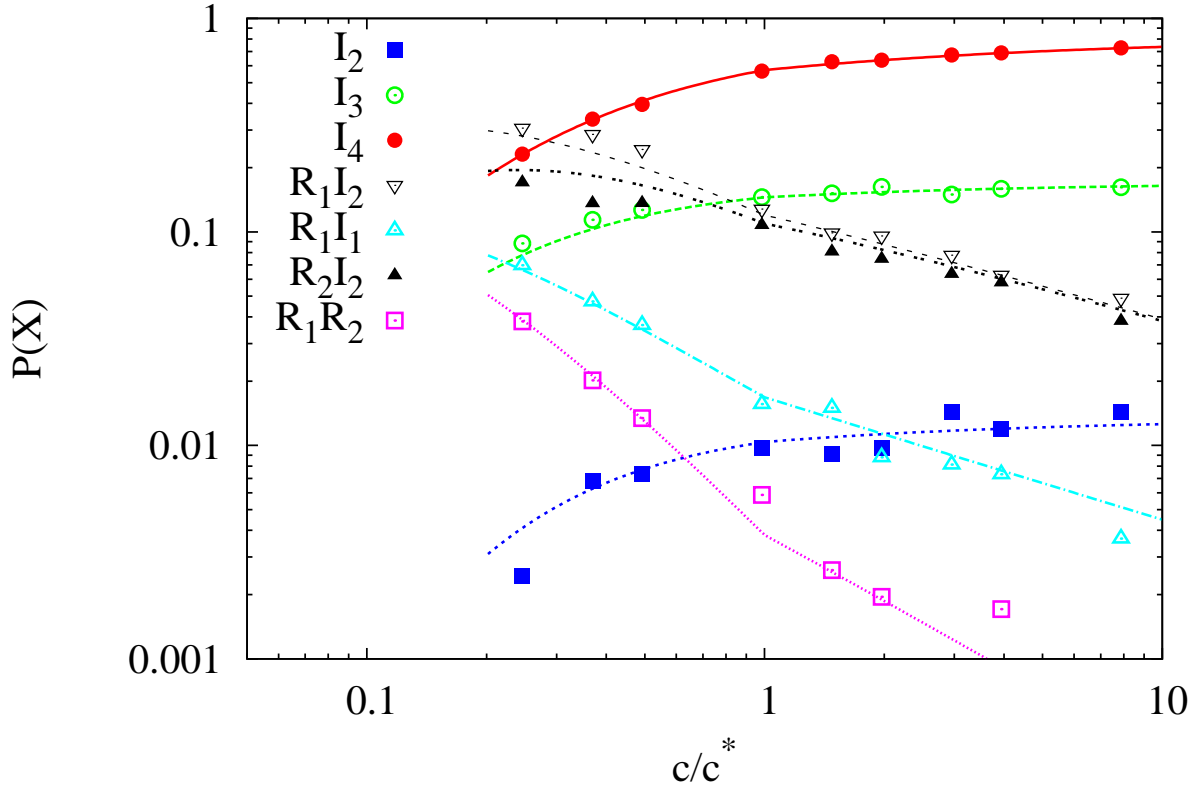


FIGURE 3.1. Frequency of occurrence of frequent star connectivities as function of concentration for A networks. Data points: simulation data, lines are obtained by numerical integration of equations (3.1) to (3.17) using $p = 0.95$ and the additional factor of $6/5$ for ring formation to match the data. The kink in the theoretical lines is due to applying different regimes for star conformations.

$$(3.16) \quad \frac{dR_2^3}{dp} = k_{2,3}R_2^2,$$

and for the stars containing loops of both types R_1 and R_2

$$(3.17) \quad \frac{dR_1R_2}{dp} = k_{1,2}R_2 + k_{2,1}R_1I_1.$$

Note that the above rate equations were written for A systems. AB systems are readily modeled by putting all reaction rates $k_{1,i} = 0$ and by computing only species that do not contain R_1 . Then, only reactions between species of the right half of the reaction diagram are taken into account.

Figure 3.1 compares the results of the numerical integration of the above rate equations with the data of the most frequent structures in the A network series. For any star connectivity, we find excellent agreement. Weak deviations are visible below the overlap concentration, which might

be caused by density fluctuations of stars in space. For loops R_2 the theory slightly overestimates loop formation. Here, the repulsion among stars and partial disinterpenetration near c^* [26] was ignored in the rate equations and the data were adjusted to fit overall formation of loops R_1 . Note that for figures 3.1-3.3 data in the range of $P(X) = 0.001$ refers to single events per sample. Due to the limited number of about 4000 stars per sample, the relative error for the data is of order $[4000 \cdot P(X)]^{-1/2}$. Therefore, the data of Figure 3.1 suggest that the above mean-field approximation is well suited to describe the distribution of the predominant reactive species in f -functional homopolymerizations at concentrations from c^* up to melt conditions.

The same parameters for loop formation as for A networks can be chosen to compare with AB co-polymer networks. Due to the stoichiometry of the samples, the total density of reactive groups is twice the density of reactive A or B groups, and thus, the formation of loops of same size as in A networks is roughly doubled in AB networks. Since A reacts exclusively with B, there are only rings containing an even number of molecules possible. Figure 3.2 compares our predictions with the simulation data. Here, composition fluctuations of the local volume fractions of A and B species freeze in upon cross-linking and lead to regions with fluctuating conversion, depending on the local stoichiometry of the species [11]. This is also indicated at Figure 2.2: within the black circle, there is a larger number of red molecules, which leads to a local imbalance of reactive groups. Interestingly, these fluctuations leave the formation of loops R_2I_2 mainly unaffected. The reason for this observation is that loops R_2 are formed between A and B and thus (as all reacted groups) are part of the homogeneously distributed A and B groups, while the remaining unreacted dangling arms at high conversion are mainly in volumes with non-stoichiometric distribution of A and B groups. Therefore, the frequency of connectivities that are incompletely reacted is mainly affected by local fluctuations of A vs. B reactive groups. The deviations between simulation data and theoretical prediction indicate that mean-field estimates for co-polymerizations need to be improved to take into account the effect of composition fluctuations of the different species. These fluctuations depend strongly on mixing and total reaction rate [11] and should show a clear dependence on the functionality of the molecules.

The species R_2R_2 , R_2^3 , and $R_2^2I_1$ have an additional dependence on the number of existing bonds between a pair of molecules and depend strongly on the estimate of the number of un-reacted groups on connected molecules. Therefore, the data on these structures is the best choice for testing equation (2.2) and (2.9). Figure 3.3 shows that our computations yields a rather good over

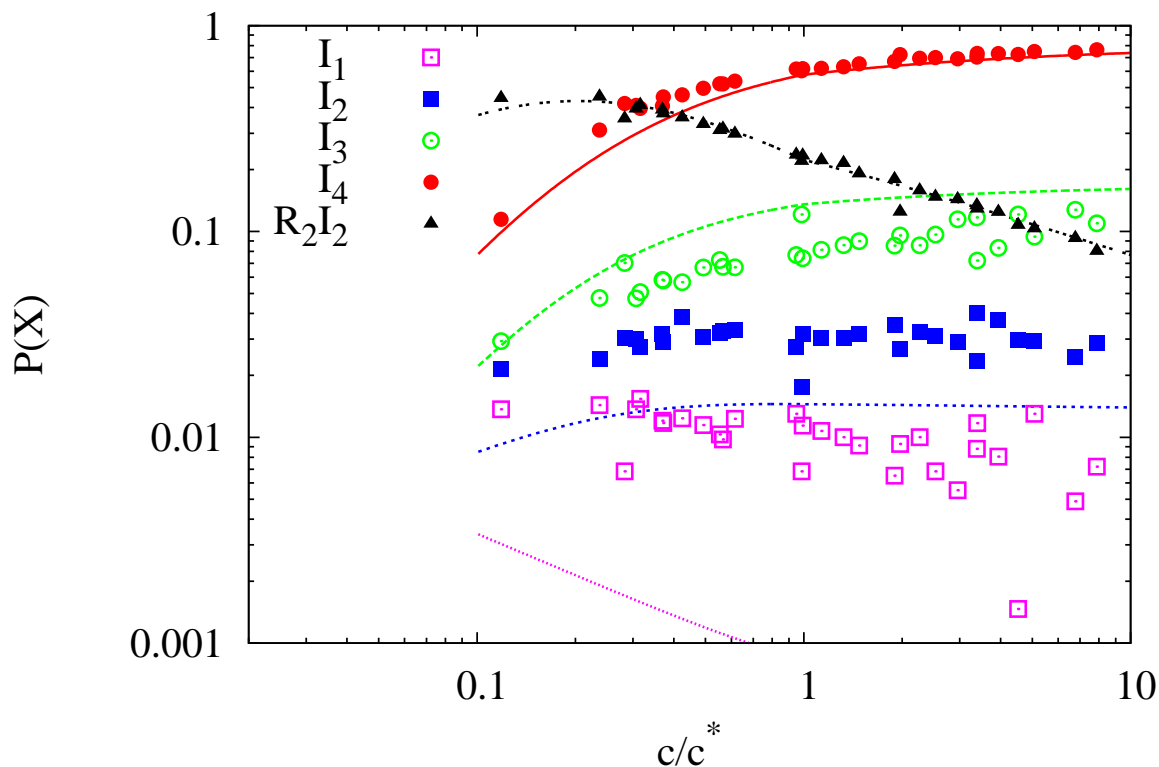


FIGURE 3.2. Frequency of occurrence of the most predominant star connectivities as function of concentration for AB networks. Simulation data (data points) and computation (lines) using the same (fit-)parameters as in Figure 3.1 and considering the smaller density of A and B groups.

all agreement for all species that have four arms reacted. Species containing rings with less than four reacted arms show quantitatively the same shift in the frequency of occurrence as the species I_j with the same number of reacted arms $j < f$ in Figure 3.2. As an example we included the most frequent species R_2I_1 . Note that species R_2^3 leads to an extra amount of sol that is exclusively made of short cycles.

In contrast to previous work [20, 9, 1, 24], the simulations of our work explicitly model conformations and dynamics of all monomers by taking into account excluded volume, entanglements and the embedding of the monomers in space. Reactions occur on the course of motion and collision of reactive groups in space. Therefore, the data of our simulations are independent of the mean field assumptions made for computing the rate equations and thus, serve as a critical test of our approach. The good agreement between data and theory shows that our approach is suitable to describe the short range connectivity based on a nearest neighbour analysis. The above detailed

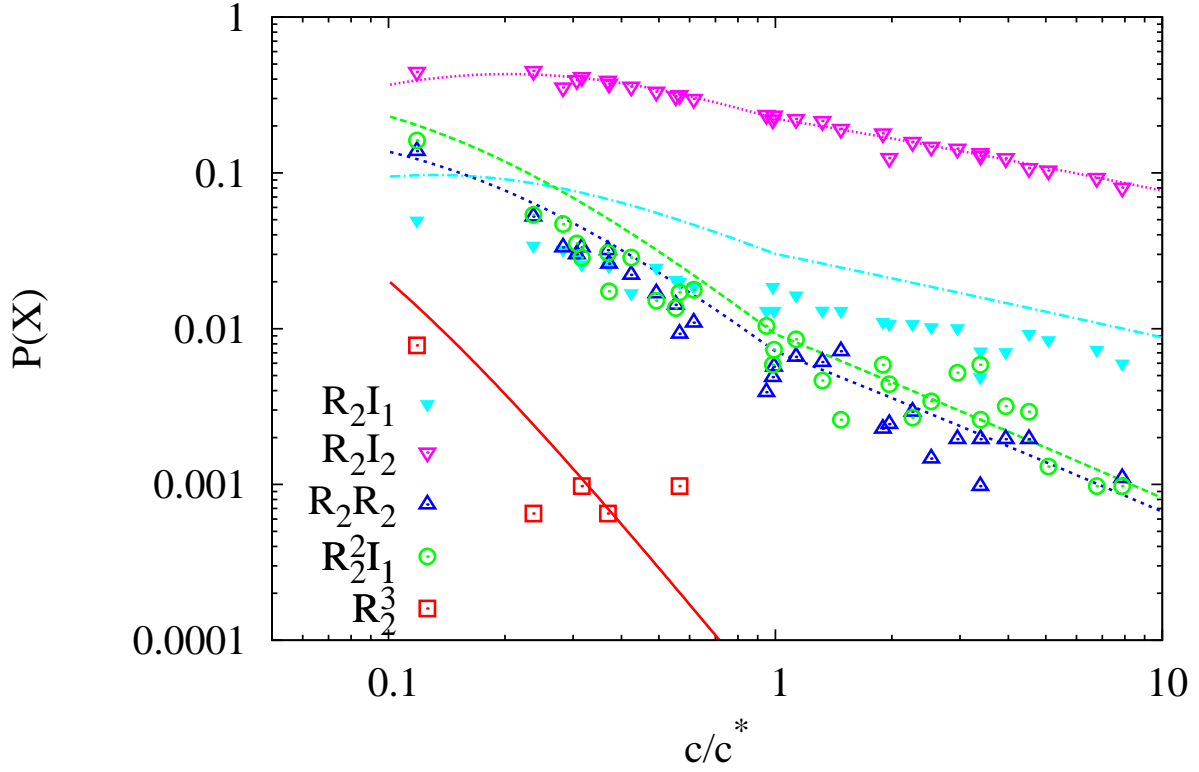


FIGURE 3.3. Frequency of occurrence of star connectivities R_2I_2 , R_2R_2 , $R_2^2I_1$, and R_2^3 with four reacted arms in AB networks. The connectivity R_2I_1 (full symbols) contains one unreacted arm and is shifted with respect to the theoretical predictions similar to I_3 (see Figure 3.2).

analysis of short loops in networks also reveals that for both A and AB networks the loops R_1 and R_2 (if existing) are dominating for the parameters of the present study. More complicated loop-structures that may have a different concentration dependence, see Figure 3.1 to 3.3 are clearly less pronounced but become important for very low concentrations. Therefore, the simple scaling approach in our previous work [26] is justified to approximate the total amount of loops in the samples for the current set of parameters. We further note that the simulation results of our proceeding work were in good qualitative agreement with recent experimental data [14]. Therefore, we assume that the present study is fundamental for a detailed analysis of the structure of these four arm star tetra-PEG networks.

4. BRANCHING DISTRIBUTIONS AND NETWORK PROPERTIES

Above we showed that our approach is suitable to describe the formation of short loops in the networks. The elasticity of a polymer strand, however, depends on the global embedding of this strand into the network structure. Therefore, we test in the current section, whether our mean-field description of short cyclic defects is sufficient to conclude for the global structure of the networks that manifests itself, for instance, in the amount of active material.

According to the definition of the connectivities in Figure 2.1, the mole fractions of stars a_i which can have i connections to the incipient gel is given by

$$(4.1) \quad a_0 = I_0 + R_1^2 + R_2^3 + R_1$$

$$(4.2) \quad a_1 = I_1 + R_1 R_2 + R_2 + R_1 I_1 + R_2^2$$

$$(4.3) \quad a_2 = I_2 + R_1 I_2 + R_2^2 I_1 + R_2 R_2 + R_2 I_1$$

$$(4.4) \quad a_3 = I_3 + R_2 I_2$$

$$(4.5) \quad a_4 = I_4.$$

The distribution of mole fractions a_i is the key quantity to operate with the work of Miller & Macosko [17]. In our approach, we consider a cyclic structure R_1 as a reduction of the functionality by 2 and loops R_2 as reductions of the effective functionality by 1 as used in the above equations. For connectivity R_2^3 we consider that these species can only be part of sol for $f = 4$.

Let $P(F_A^{out})$ denote the probability of finding a finite chain starting at a randomly selected arm. Then we can write following the ideas of Ref. [17]

$$(4.6) \quad P(F_A^{out}) = pP(F_A^{in}) + 1 - p$$

and

$$(4.7) \quad P(F_A^{in}) = \sum_i a_i P(F_A^{out})^{i-1}.$$

Since $P(F_A^{out}) = 1$ is always a solution, the desired root² to solve the above set of equations is

$$(4.8) \quad P(F_A^{out}) = -\frac{a_3}{2a_4} - \frac{1}{2} + \left(a_3^2 - a_4(3a_4 + 2a_3 + 4a_2 - 4/p')\right)^{1/2} / 2a_4,$$

provided that this solution is between 0 and 1. Since above we included also incompletely reacted stars into the distribution a_i and we are only concerned with stoichiometric samples here, we can put $p' = 1$.

The probability that a unit of $0 \leq i \leq f$ potential connections has $k \leq i$ bonds that are not finite is given by the binomial distribution

$$(4.9) \quad P(X_{k,i}) \approx \binom{i}{k} P(F_A^{out})^{i-k} (1 - P(F_A^{out}))^k.$$

Note that the equation above is exact, if there are no correlations among different types of connected stars. Since rings of type R_2 always introduce correlations among the functionalities of connected stars, we implicitly test below by comparing with simulation data whether ignoring these local correlations is a good approximation for global connectivity, since the simulation results are subject to these correlations.

In the classical definition of the active material by Scanlan [25] and Case [3], the global connectivity of a given branching point is analyzed: If there are at least three independent paths to the network, the branching point is called active and any chain (or series of chains) connecting two active branching points is part of the elastically active material. Any part of the network that is attached to the rest of the sample by only one connection contributes to the elastically inactive “dangling” material. Thus, for estimating the amount of active material, we have to first compute the number fraction of stars that have exactly k non-finite independent connections to gel:

$$(4.10) \quad X_k = \sum_{i=k}^f A_i P(X_{k,i}).$$

These number fractions are shown in Figure 4.1 and 4.2 for A and AB networks respectively. In our approach we consider only R_1 and R_2 formation and neglect correlations among rings and density fluctuations of stars in space. Therefore, the estimates for the gel point (as suggested by

²Note that the first term of the solution is missing at equation (24) of Ref. [17].

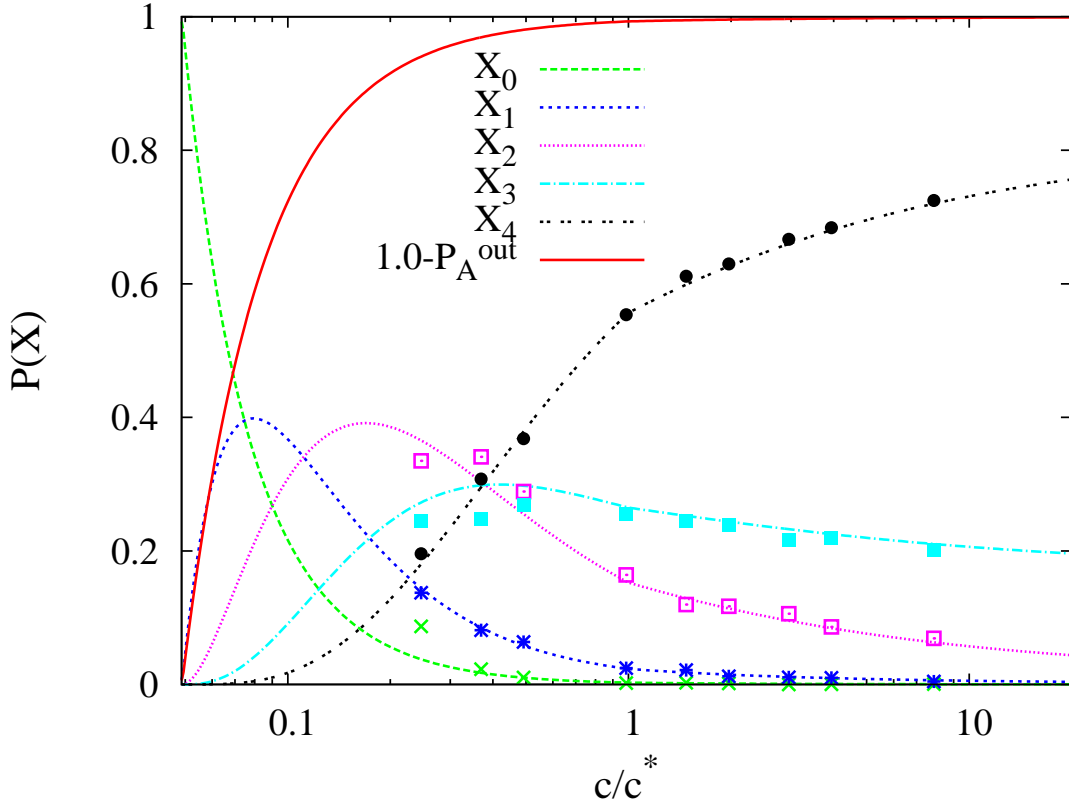


FIGURE 4.1. Number fractions of stars X_i with i independent paths to the incipient gel for A networks of $f = 4$ at $p = 0.95$ (data points) compared with the theoretical prediction.

the intersection of the probability of finding an infinite chain starting at a randomly selected arm, $(1 - P_A^{\text{out}})$ and the x -axis) are lower boundaries for the gel point and the distributions clearly below c^* have to be considered with care. Note that the kinks in the distribution function are due to different approximations above and below the overlap concentration (cf. equation (2.2) and (2.3)).

The data for the A networks in Figure 4.1 are in rather good agreement with the theoretical predictions. Therefore, we conclude that correlations among the functionalities of connected stars can be ignored in first approximation. Concentration fluctuations of stars, as for instance important for the increased formation of X_0 below c^* are more important to be considered. The data of the AB networks in Figure 4.2 shows on the other hand, that the changes in the local connectivity caused by concentration fluctuations of A and B stars also lead to a systematically modified global connectivity. Additionally, using an AB type reaction leads to a large shift of the predicted minimum

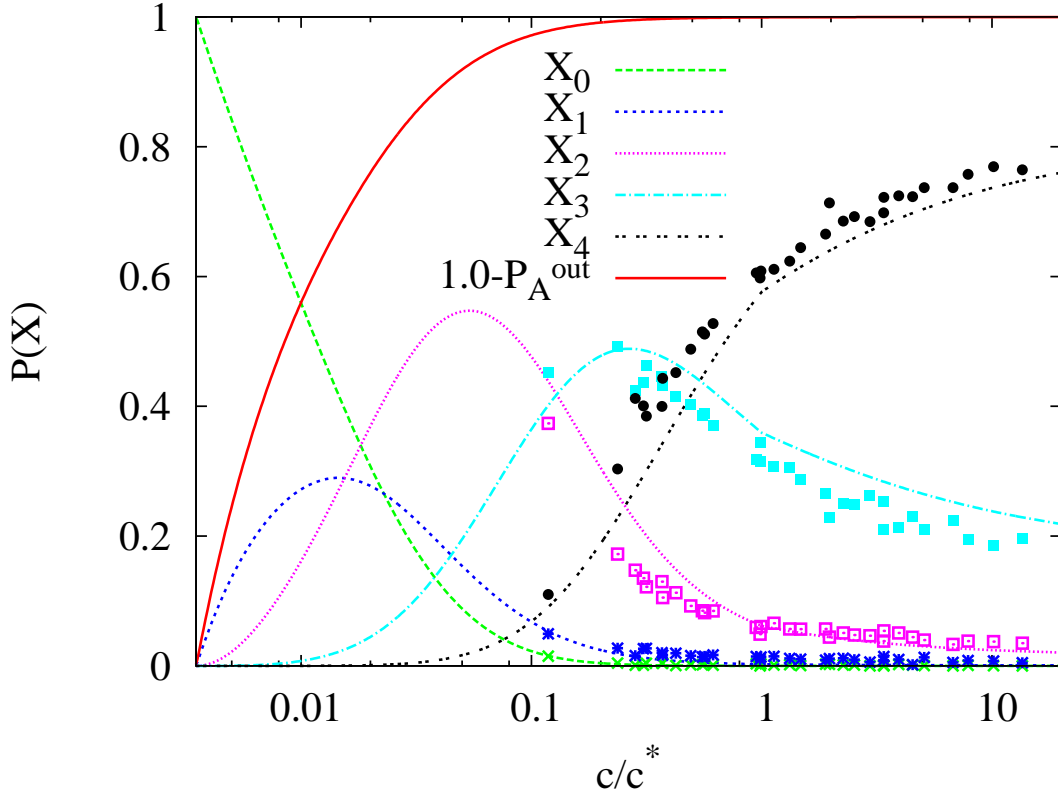


FIGURE 4.2. Number fractions of stars X_i with i independent paths to the incipient gel for AB networks of $f = 4$ at $p = 0.95$ (data points) compared with the theoretical prediction.

concentration for gel formation at $p = 0.95$ as compared to A networks. This is mainly caused by the absence of loops R_1 .

Next, we analyze the weight fractions of sol, the active, and the dangling material. The weight fraction w_a of active material among all polymer is the weight fraction of effective strands

$$(4.11) \quad w_e = \sum_{i=2}^f iX_i/f$$

plus one additional strand per loop R_2 inside the active material. Thus, we have to consider the remaining connections attached to the loop(s) between the two stars in order to estimate whether this loop is active or not. The additional active material stored in loops R_2 is, therefore, given by

$$(4.12) \quad w_{R_2} \approx P(X_{2,2})R_2I_1/4 + P(X_{3,3})R_2I_2/4 \\ + P(X_{2,3})R_2I_2/6 + P(X_{2,2})2R_2I_1/2 + P(X_{2,2})R_2R_2)/2.$$

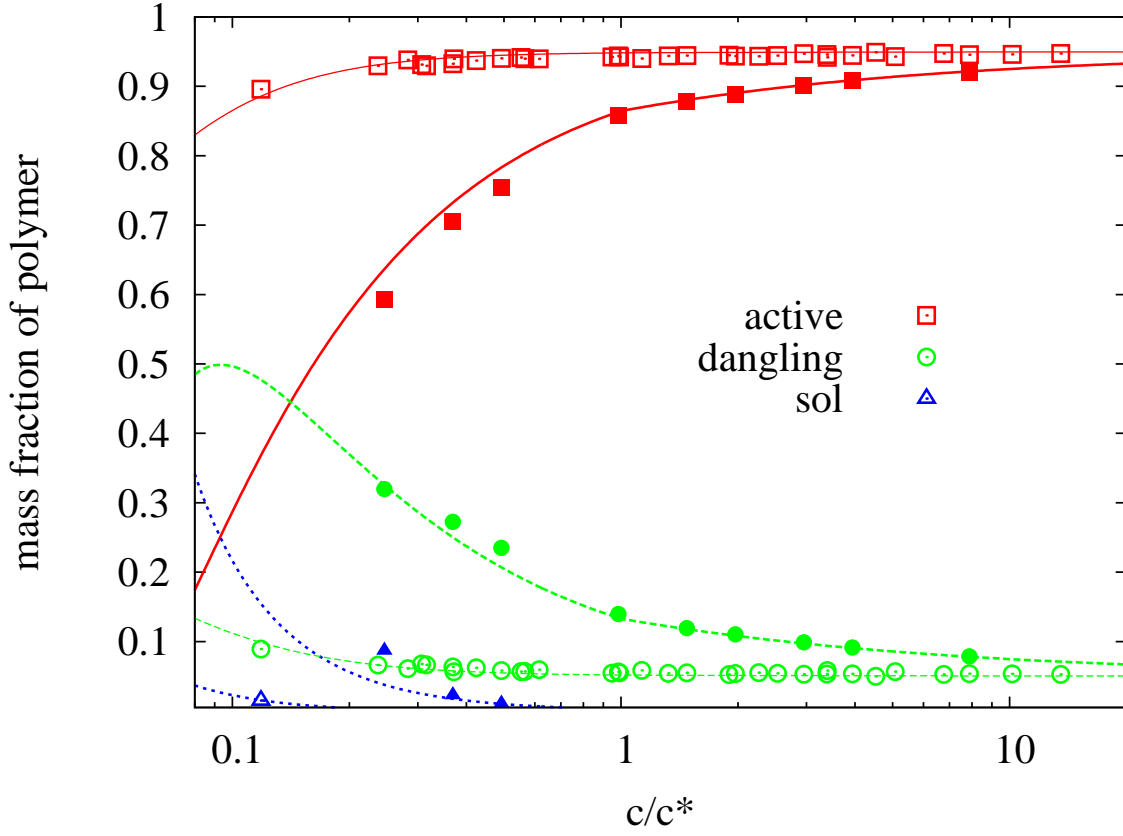


FIGURE 4.3. Polymer mass fractions of dangling material (circles), sol (triangles), and active material (squares) of A (full symbols) and AB networks (hollow symbols) as function of concentration. Thick lines represent estimates for A networks, thin lines for AB networks.

The total amount of the active material is then

$$(4.13) \quad w_{act} = w_e + w_{R_2}.$$

Note that $2w_{R_2}/w_{act}$ is, therefore, the weight fraction of loops R_2 inside the active material.

According to our definitions,

$$(4.14) \quad w_{sol} = A_0$$

and therefore, the weight fraction of dangling material can be computed as

$$(4.15) \quad w_{dangl} = 1 - w_{act} - w_{sol}.$$

The amount of active and dangling material as well as sol is shown in Figure 4.3 for A and AB networks. The striking result of this analysis is that even at concentrations of $c^*/10$ nearly all polymer material is active for the AB networks in large contrast to A networks. This stems from the fact that loops R_1 are missing in AB networks and the predominant non-ideality of network structure is the formation of loops R_2 which effectively leads to a reduction of average functionality (here from 4 to 3) but otherwise no impact on the amount of the active material. Note that this observation requires $f \geq 4$. Over all, Figure 4.3 suggests that the network stability is nearly constant over a wide range of c , if the same conversion p was achieved among all samples. Therefore, this result is in striking agreement with the nearly constant breaking strain as observed in the experiments of Sakai [22]. However, multiple links lead to a reduction of the average effective functionality of the stars and thus, to a modification of phantom modulus different to changes in the amount of the active material as discussed in the following section.

5. APPLICATION TO NETWORK ELASTICITY

Flory already argued [6], that finite cycles would diminish the elastic response of the network. This effect is most pronounced for the shortest non-dangling rings and ignorable for larger ring sizes, since the computation of the cross-link fluctuations runs over a geometric series, which quickly converges against its asymptote. In fact, the derivation of the phantom modulus

$$(5.1) \quad G_{ph,id} = \frac{f-2}{f} \cdot \nu k_B T = \frac{f-2}{f} \cdot \frac{k_B T}{v_{mon} N}$$

for ideal f -functional networks without defects requires the assumption that all cycles are closed at infinity [6]. Here, ν is the number density of network strands, k_B the Boltzmann constant, T temperature, and v_{mon} the volume of a monomer.

As compared to this ideal prediction, short loops inside the active network structure will reduce the phantom modulus, even though these rings are still actively deformed. In the discussion of Flory [6], a correction for these short circuits was omitted due to the large overlap number, $P \gg 1$, of active strands in networks crosslinked at $c \gg c^*$, which reduces their frequency of occurrence. However, this argument is questionable for polymer gels close to overlap concentration c^* , for which only a small number of neighboring molecules exist.

In the following, we estimate the phantom modulus by using the number average strand length N_{av} and weight average active junction functionality $\langle f_a \rangle$. Thereto, we interpret multiple links as

single connection of reduced degree of polymerization between the same two star centers: a double link R_2 effectively deforms as a single chain of $N/2$ monomers, while a triple link R_2^2 deforms like a chain of $N/3$ monomers. A linear series of two double links behaves like a single chain of N monomers, and so on. Since the effect of R_2^2 and a series of two double links is rather small and almost mutually cancelling for most samples of our study, we approximate the effect of multiple links onto average strand lengths by replacing a fraction of w_{R_2}/w_{act} active connections with chains of $N/2$ monomers. This leads to an average strand length of roughly $[1 - w_{R_2}/2w_{act}]N$ monomers, whereby w_{act} is the weight fraction of active strands and w_{R_2} half the weight fraction of the loops R_2 inside the active material (cf. section 4 for the computation of w_{act} and w_{R_2}). 2-functional junctions as caused by dangling loops for $f = 4$ on the other hand effectively dilute the concentration of branching points inside the active material by a factor

$$(5.2) \quad \alpha = \sum_{k=2}^i X_k / \sum_{k=3}^i X_k.$$

Here, X_k is the number fraction of units with k non-finite connections to the gel. The average active network strand is therefore

$$(5.3) \quad N_{av} \approx \alpha[1 - w_{R_2}/2w_{act}]N.$$

and the average active functionality for $f = 4$ is given by

$$(5.4) \quad \langle f_a \rangle = (3X_3 + 4X_4)/(X_3 + X_4).$$

Both expressions for N_{av} and $\langle f_a \rangle$ then replace N and f at equation (5.1).

To decide whether $\langle f_a \rangle$ of N_{av} is playing the leading role for the effect on modulus depends to a large extent on whether it is an A or an AB network, in particular for small $f = 3, 4$. For our series of data, the modification of N_{av} and the reduction in the concentration of active junctions are responsible for the reduction of the modulus of A networks above c^* , while below c^* the average functionality of active junctions is increasingly affected for A and AB networks.

G_{ph} was computed independently for the network structures of the simulations and for the solutions of the rate equations of section 3. The result of this computation as shown at Figure 5.1 indicates that the above estimate agrees well with the data on the homopolymer networks and thus, correlations among multiply connected molecules can be neglected for these samples. The effect of

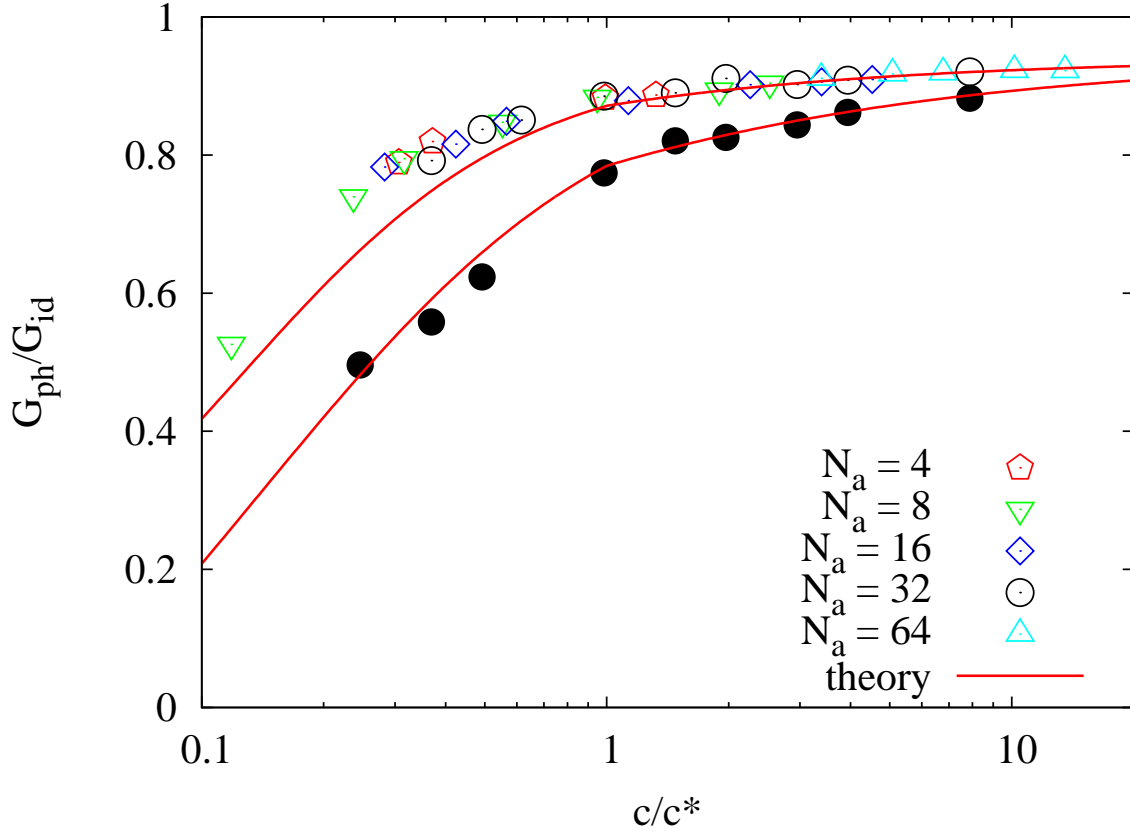


FIGURE 5.1. The reduction of phantom modulus after consideration of rings R_2 and R_1 as function of the overlap number of stars c/c^* . Hollow symbols show the data of AB networks, full symbols data of A networks. Data is normalized by the ideal phantom modulus G_{id} of a 4-functional network at same density.

fluctuations is still clearly visible for the AB networks. Furthermore, we observe a clear drop of the phantom modulus of AB networks as compared to ideal network structures starting at c^* to lower concentrations. This drop sets in at much higher conversions as the drop of the amount of active material, since it is mainly caused by the reduction of the average functionality of the molecules.

6. SUMMARY

We have presented a rate theory approach to describe network formation of f -functional stars including the effect of short loops. We showed that the only parameter for all computations is the ratio of $k_{1,f-2}(c^*)/k_{0,f-1}(c^*)$ (i.e. single pair intra-molecular vs. single pair inter-molecular reaction rate), since all other reaction rates are functions of one of these two reaction rates. This ratio is well approximated by the ratio of the gyration volume and the accessible volume of star arms R_g^3/R_e^3 up to a numerical fit-factor of 6/5 for the data of our study. The concentration dependence of the

reaction rates is in rather good agreement with the scaling of the conformations of the molecules. The observed small change of the scaling of loop formation as function of concentration was attributed to a partial disinterpenetration of the molecules, which has not yet been considered by theory. Agreement between data and theory, thus, justifies the neglect of diffusion for the discussion of network formation for networks of four-arm stars. This observation is in agreement with a recent experimental study on reaction kinetics[18], which observed no effects of steric hindrance or the gelation threshold, which both are related to diffusion.

For the samples of our study, we could not find significant differences as function of reaction rate. Therefore, it might be possible to ignore the effect of dynamics on the structure of networks of star molecules, if these were obtained from homogeneously mixed samples. The comparison of the theoretical predictions with simulation data on homopolymer A networks reveals that correlations among molecules can be ignored. Also, for concentrations $c > c^*/4$ the effect of local fluctuations of polymer density can be ignored and mean-field descriptions can be rather precise for computing the amount of short cyclic structures inside the networks, as we can judge from the data of the present work.

Co-polymer networks made by exclusively reacting A with B species on the other hand show a clear effect of composition fluctuations that leads to fluctuations of the reactive groups of one species in space, even though the total density of polymers might be equilibrated. Mean-field descriptions of these samples are therefore less accurate. Furthermore, experimental data is expected to be very sensitive with respect of mixing both types of molecules. The data of the present study does not allow to look with more detail into this problem, since the main parameters for this effect are a) a amplitude of the initial composition fluctuation, b) a variation of the over all reaction rate, c) the functionality of the molecules. But our results suggest that a systematic study will be essential for understanding the differences between homo-polymer and co-polymer networks. The results for the total amount of active material suggest a much more stable network structure for very low concentrations in the case of AB-networks as compared to homopolymer networks at same conversion. Apparently, this effect arises from the missing R_1 loops in AB networks. But the modulus of the networks is expected to show a stronger dependence on decreasing concentration at $c < c^*$ in case of AB networks, since there, first the functionality of the molecules is reduced before the amount of active material is lowered.

Finally, the striking differences between A and AB networks (and between these samples and ideal networks) exemplify the importance of understanding of network formation: even though the building blocks of the network are of identical structure, the condition of linking exclusively A with B groups implies clearly different network structures and thus, material properties.

7. ACKNOWLEDGEMENT

The authors thank the ZIH Dresden for a generous grant of computing time. ML thanks the DFG for funding project LA2735/2-1.

REFERENCES

- [1] E. Ben-Naim and P.L. Krapivsky. Kinetics of ring formation. *Phys. Rev. E*, 83:061102, 2011.
- [2] J.I. Cail, R.F.T. Stepto, and D.J.R. Taylor. Formation, Structure and Properties of Polymer Networks: Gel-Point Prediction in Endlinking Polymerisations. *Macromol. Symp.*, 171:19–36, 2001.
- [3] L.C. Case. Branching in polymers. I. Network defects. *Journal of Polymer Science*, 45(146):397–404, 1960.
- [4] K. Dusek, M. Gordon, and S.B. Ross-Murphy. Graphlike State of Matter. 10. Cyclization and Concentration of Elastically Active Network Chains in Polymer Networks. *Macromolecules*, 11:236–245, 1978.
- [5] K. Dusek and V. Vojta. Concentration of Elastically Active Network Chains and Cyclisation in Networks Obtained by Alternating Stepwise Polymerization. *Brit. Polym. J.*, 9:164–171, 1977.
- [6] P.J. Flory, M. Gordon, and N.G. McCrum. Statistical thermodynamics of random networks [and discussion]. *Proceedings of the Royal Society of London. Series A, Mathematical and Physical Sciences*, 351(1666):351–380, 1976.
- [7] M. Gordon and G.R. Scantlebury. *J. Pol. Sci. C*, 16:3933, 1968.
- [8] S. Kuchanov, H. Slot, and A. Stroeks. Development of a quantitative theory of polycondensation. *Prog. Polym. Sci.*, 29:563–633, 2004.
- [9] D.L. Kurdikar, J. Somvarsky, K. Dusek, and N.A. Peppas. Development and Evaluation of a Monte Carlo Technique for the Simulation of Multifunctional Polymerizations. *Macromolecules*, 28:5910–5920, 1995.
- [10] M. Lang. *Bildung und Struktur von polymeren Netzwerken*. PhD thesis, Universität Regensburg, 2004.
- [11] M. Lang, D. Göritz, and S. Kreitmeier. The effect of spatially inhomogeneous mixing of polymer and cross-links for end-linked polymer networks. In *Constitutive models for rubber III: proceedings of the Third European Conference on Constitutive Models for Rubber, 15-17 September 2003, London, UK*, page 195. Taylor & Francis, 2003.
- [12] M. Lang, D. Göritz, and S. Kreitmeier. Intramolecular Reactions in Randomly End-Linked Polymer Networks and Linear (Co) polymerizations. *Macromolecules*, 38(6):2515–2523, 2005.
- [13] M. Lang and J.-U. Sommer. On the origin of the scattering of gels and swollen polymer networks. In *CONSTITUTIVE MODELS FOR RUBBER-PROCEEDINGS-*, volume 5, page 147. Balkema, 2008.

- [14] F. Lange, K. Schwenke, M. Kurakazu, Y. Akagi, U. Chung, M. Lang, J.-U. Sommer, T. Sakai, and K. Saalwächter. Connectivity and Structural Defects in Model Hydrogels: A Combined Proton NMR and Monte Carlo Simulation Study. *Macromolecules*, 44:9666–9674, 2011.
- [15] S. Lay, J.-U. Sommer, and A. Blumen. Comparison of structural properties of different polymer network types as obtained by computer simulation. *The Journal of Chemical Physics*, 110:12173, 1999.
- [16] Y.-K. Leung and B.E. Eichinger. Computer simulation of end-linked elastomers. I. Trifunctional networks cured in the bulk. *J. Chem. Phys.*, 80:3877–3884, 1984.
- [17] D.R. Miller and C.W. Macosko. A new derivation of post gel properties of network polymers. *Macromolecules*, 9(2):206–211, 1976.
- [18] K. Nishi, F. Fujii, M. Chijiishi, Y. Katsumoto, U. Chung, T. Sakai, and M. Shibayama. Kinetic Study for AB-Type Coupling Reaction of Tetra-Arm Polymers. *Macromolecules*, ASAP:ma202386k, 2011.
- [19] S. Pereda, A. Brandolin, E.M. Valles, and C. Sarmoria. Copolymerization between A_3 and B_2 with Ring Formation and Different Intrinsic Reactivity in One of the Monomers. *Macromolecules*, 34:4390–4400, 2001.
- [20] S.E. Rankin, L.J. Kasehagen, A.V. McCormick, and C.W. Makosko. Dynamic Monte Carlo Simulation of Gelation with Extensive Cyclization. *Macromolecules*, 33:7639–7648, 2000.
- [21] M. Rubinstein and R. Colby. *Polymer Physics*. Oxford University Press, New York, NY, United States of America, 2003.
- [22] T. Sakai, T. Matsunaga, Y. Yamamoto, C. Ito, R. Yoshida, S. Suzuki, N. Sasaki, M. Shibayama, and U. Chung. Design and Fabrication of a High-Strength Hydrogel with Ideally Homogeneous Network Structure from Tetrahedron-like Macromonomers. *Macromolecules*, 41(14):5379–5384, 2008.
- [23] C. Sarmoria and D.R. Miller. Spanning-tree models for AF homopolymerizations with intramolecular reactions. *Comput. Theo. Pol. Sci.*, 11:113–127, 2001.
- [24] C. Sarmoria, E.M. Valles, and D.R. Miller. Validity of Some Approximations Used to Model Intramolecular Reaction in Irreversible Polymerization. *Macromolecules*, 23:580–589, 1990.
- [25] J. Scanlan. The effect of network flaws on the elastic properties of vulcanizates. *Journal of Polymer Science*, 43(142):501–508, 1960.
- [26] K. Schwenke, M. Lang, and J.-U. Sommer. On the Structure of Star-Polymer Networks. *Macromolecules*, 44:9464–9472, 2011.
- [27] J.L. Stanford and R.F.T. Stepto. . *J. Chem. Soc. Faraday Trans.*, 1(71):1292–1307, 1975.
- [28] J.L. Stanford, R.F.T. Stepto, and D.R. Waywell. . *J. Chem. Soc. Faraday Trans.*, 1(71):1308–1326, 1975.
- [29] R.F.T. Stepto, J. Cail, and D. Taylor. Formation, Structure and Properties of Polymer Networks: Theory and Modelling. *Macromol. Symp.*, 183:165–172, 2002.
- [30] K. Suematsu. Recent Progress in Gell Theory: Ring, Excluded Volume, and Dimension. *Advances in Polymer Science*, 156:137–214, 2002.
- [31] H.L. Trautenberg, J.-U. Sommer, and D. Göritz. Structure and swelling of end-linked model networks. *Journal of the Chemical Society*, 91(16):2649–2653, AUG 21 1995.

TABLE OF CONTENTS GRAPHIC

Reaction Diagram

Michael Lang

Konrad Schwenke

Jens-Uwe Sommer

Homopolymer
networks

Homopolymer **and**
Copolymer networks

